SAND2019-5751J

Pilot-scale open raceway ponds and flat-panel photobioreactors maintain well-mixed conditions under a wide range of mixing energy inputs

Carlos Quiroz-Arita[1], Myra L. Blaylock[2], Patricia E. Gharagozloo[3], David Bark[1], Lakshmi Prasad Dasi[4], Thomas H. Bradley[1]

[1]Mechanical Engineering, Colorado State University, Fort Collins, CO 80524, USA

[2]Sandia National Laboratories, Livermore, CA 94551, USA

[3] Lawrence Livermore National Laboratory, Livermore, CA 94550, USA

[4]Department of Biomedical Engineering, The Ohio State University, Columbus, OH 43210, USA

Corresponding author:

Name: Carlos Quiroz-Arita

Address: Idaho National Laboratory 1955 N. Fremont Avenue, Idaho Falls, ID 83415

E-mail address: carlos.quiroz@fulbrightmail.org

Phone: +1 (970) 215-1583

Short running title:

Pilot photobioreactors maintain well-mixed conditions

Abstract

Turbulent mixing in pilot-scale cultivation systems is hypothesized to influence the productivity of photoautotrophic cultures. We studied turbulent mixing by applying particle image velocimetry (PIV) and acoustic doppler velocimetry (ADV) to pilot scale flat-panel photobioreactors and open raceway ponds. Mixing energy inputs were varied from 0.03 to 1.97 $W \cdot m^{-3}$. The experimental results were used to quantify turbulence and to validate computational fluid dynamics (CFD) models, from which Lagrangian representations of the fluid motion in these reactors was derived. The results of this investigation demonstrate that differences in mixing energy input do not significantly impact the structure of turbulence in the reactors, nor the frequency of photoautotrophic microorganisms' motions within the reactors. The experimental and computational results of our research demonstrate that well-mixed conditions exist in pilot flat-panel photobioreactors and open raceway ponds, even at relatively low mixing energy inputs.

Keywords:

Mixing energy, dark/light cycles, open raceway pond, flat-panel photobioreactor, fluid mechanics

1. Introduction

Photoautotroph-based biofuels are considered one of the most promising renewable fuels to meet the global energy requirements for transportation systems (Y. Chisti, 2007). Long-term research and development has resulted in demonstrations of microalgae areal oil productivities that are higher than crop-based biofuels, about 10 times that of palm oil and about 131 times that of soybean (Brune, Lundquist, & Benemann, 2009; Y. Chisti, 2007; Lardon, Helias, Sialve, Steyer, & Bernard, 2009; Rodolfi et al., 2009). Cyanobacteria is reported to have ~4 times the areal productivity of microalgae on an equivalent energy basis (Robertson et al., 2011). Downstream of this cultivation process, cyanobacterial biomass and bioproducts can be supplied to biorefineries producing feed, biomaterials, biosynthetic chemicals, and biofuels (Wijffels, Kruse, & Hellingwerf, 2013). As such, cyanobacteria-based biofuel systems may be a significant contributor to more sustainable energy and material production systems.

Turbulent cultivation environments have been demonstrated to induce physiological responses in photoautotrophic microorganisms in open raceway ponds and photobioreactors (Fadlallah et al., 2016; Havens, James, East, & Smith, 2003; Kumar, Dasgupta, Nayak, Lindblad, & Das, 2011; Michels, van der Goot, Norsker, & Wijffels, 2010; Mirón et al., 2003; Moisander, Hench, Kononen, & Paerl, 2002; Nguyen & Hoang, 2016; Xiao, Li, Li, Zhang, & Guo, 2016). For example, recent efforts studied the effects of turbulence dissipation rates ranging from 0 to $8E^{-2}$ $m^2.s^{-3}$ simulated at laboratory scale conditions (1-liter cultures) (Xiao et al., 2016). This work concluded that despite no alteration of photosynthesis activity (as measured by chlorophyll a), there is a systematic increase in the growth rates of the strain *Microcystis flos-aquae* as a function of the turbulent dissipation rate, and a decrease in the growth rate of the strain *Anabaena flos-aquae* at high turbulence. These authors identified that a maximum phosphorous

uptake rate in these cyanobacteria strains occurs at turbulence dissipation rates of $2.26E^{-2}$ $m^2.s^{-3}$, suggesting that turbulence plays an important role in the biological adaptation of cyanobacteria by influencing nutrient uptake (Xiao et al., 2016). In other recent research, the effects of shear environments were studied for the cyanobacteria and microalgae strains *Synechocystis sp.* and *Chlamydomonas reinhardtii*, in 150 ml cultures (Fadlallah et al., 2016). In this study, the growth rate of *Synechocystis sp.* was independent of shear stress (0 to 0.18 $N.m^{-2}$) and *Chlamydomonas reinhardtii* growth rate increased linearly with shear stress. It is an open question as to whether these research results under laboratory scale environments (<1L cultures) are representative of industrial-scale (>1000L) cultivation conditions.

Detrimental impacts of turbulent mixing have also been demonstrated, with inhibition attributed to cell disruption from shear stress (Chalmers, 2015; Han & Yuan, 2004; Kunnen, Malas, Semeins, Bakker, & Peters, 2017; Richardson, Lannigan, & Macara, 2015; Sieck et al., 2014; Sieck et al., 2013; Wang, Lü, Mao, & Long, 2014; Yi et al., 2010). For example, hybridoma cells suffer apoptosis at mixing energy inputs of $1.87E^3$ $W.m^{-3}$ (Al□Rubeai, Singh, Goldman, & Emery, 1995; Chalmers, 2015). Other studies observed 51% lower recombinant protein production, 42% higher glucose uptake, and 50% lower lactate production in cells exposed to mixing energy inputs of $6.4E^2$ $W.m^{-3}$ (Chalmers, 2015; Keane, Ryan, & Gray, 2003). In general, these inhibitory effects are reported at mixing energy inputs above $1E^6$ $W.m^{-3}$ and Kolmogorov microscales less than or equal to 2.4 micrometers for mammalian cells (Chalmers, 2015). In photobioreactors, small bubbles are reported to cause cell damage (Barbosa & Wijffels, 2004; Mirón et al., 2003), colliding with photoautotrophic cells and contributing to a high shear environment. The growth of the microalgae strain *Phaeodactylum tricornutum*, for instance, was inhibited at air rates of 0.567 $m^3_{air}.min^{-1}.m^{-3}_{reactor}$, and carboxymethyl cellulose (CMC, a

viscosity increaser) supplied into the medium had the effect of mitigating shear-induced damage in parallel experiments (Mirón et al., 2003). Other sparged photobioreactors cultivating *Dunaliella tertiolecta* and *D. salina* reported increases in the culture decay rates as a function of gas velocity, observing the highest death rates at 8.91 and 13.37 $m^3_{air}.min^{-1}.m^{-3}_{reactor}$ (Barbosa & Wijffels, 2004). There is no research reported in the literature concerning the biological system response due to shear stress on cyanobacteria cells, particularly on the biofuels-relevant strains of *Synechocystis sp.* PCC6803. Moreover, most of the previous research was conducted at mixing energy inputs that are 30, 100, or thousands order of times higher than is considered cost-effective for industrial cultivation systems (Jones, Louw, & Harrison, 2017; Sánchez Mirón, Garcia Camacho, Contreras Gomez, Grima, & Chisti, 2000).

Industrial photobioreactors are used for large-scale cultivation of photoautotrophic microorganisms, the most common types being the open raceway ponds and flat panel photobioreactors (*Microalgal Biotechnology: Potential and Production*, 2013). Open raceway ponds are constructed in a configuration with channels, using paddlewheel mixers that promote a low shear environment (Oswald, 1988). Flat-panel photobioreactors are vertically translucent flat plates, illuminated on both sides and stirred by aeration (Little, 1953). Unlike outdoor raceways and outdoor photobioreactors, laboratory-scale experiments are rigorously controlled to create ideal conditions for growth including ideal mixing rates, optimum light intensities, and optimized media, which may lead to overestimation of photoautotrophic biomass and biofuels productivity at industrial scale (Rawat, Kumar, Mutanda, & Bux, 2013). The light regime experienced by photoautotrophic microorganisms under outdoor conditions is hypothesized to be one factor in this difference in the performance of industrial systems. For instance, the light saturation of *Synechocystis sp.* PCC6803 is at about 200 μmol photons.$s^{-1}.m^{-2}$ (Kim, Vannela, Zhou, Harto, &

Rittmann, 2010; Kim, Vannela, Zhou, & Rittmann, 2011), whereas photoautotrophic microorganisms will face incident radiations of about 2000 μmol photons.s^{-1}.m^{-2} at noon in locations such as Colorado (Quinn, Turner, & Bradley, 2012). Previous studies have estimated that the total photoconversion efficiency of algae varies from between 2.6% (at high light) to 6.3% (at reduced light) (Weyer, Bush, Darzins, & Willson, 2010). These estimations assumed that 46% of the spectrum is in the photosynthetic active radiation (PAR) range of 400 to 700 nm, losses due to photon transmissions efficiency of 95%, photon utilization efficiency ranging from 10% to 30%, biomass accumulation efficiency of 50%, and biomass energy content of 21.9 kJ·g^{-1}. Low photoconversion efficiency in photoautotrophic microorganisms exposed to real-world light regimes is attributed to increased dark and photorespiration biomass losses (Drewry, Choi, An, & Gharagozloo, 2015; Edmundson & Huesemann, 2015; Gharagozloo et al., 2014).

Some previous studies have investigated the effects of mixing rates on photoautotrophic biomass productivities in industrial scale systems (Jones et al., 2017; Quinn et al., 2012; Sompech, Chisti, & Srinophakun, 2012). Some of these efforts have identified optimum volumes of air flow rates per unit volume (VVM) of photobioreactors that might be industrially relevant for microalgae, generally between 0.2 to 1.2 m^3_{air}.min^{-1}.$m^{-3}_{reactor}$ (Quinn et al., 2012). Many others have considered mixing energy inputs that are far outside the energy consumption that can be considered economic, or industrially relevant, ranging from 8 to 633 W.m^{-3} (Jones et al., 2017; Sánchez Mirón et al., 2000). For raceway ponds, for instance, energy inputs from 1 to 2 W.m^{-3} are utilized in the algae cultivation demonstrations performed to date (Sompech et al., 2012). Additionally, previous research states that mixing in industrial photobioreactors induces flashing or dark/light cycles (Janssen, Tramper, Mur, & Wijffels, 2003; Vejrazka, Janssen, Streefland, & Wijffels, 2011, 2012). For instance, by experimentally growing *Chlamydomonas*

reinhardtii under incident radiations fluctuating between 5 Hz and 100 Hz, growth rates were found to be linearly dependent on the light frequency. These previous efforts suggest that mixing in photobioreactors controls the light regimes experienced by single cells, impacting the bulk photosynthesis and biomass productivity of photoautotrophic microorganisms. However, other studies demonstrated no improvements in algal productivity at light fluctuations from 0.038 Hz to 1 Hz, modeled using a control timer to open and close a mini venetian blind device (Grobbelaar, 1991). The frequencies in these latter experiments (<< 1 Hz), are more consistent with the frequencies encountered in the circulation velocities for fermenters with a height to diameter ratio less than 3 (< 60 seconds) and for airlift reactors with split-cylinders heights of 6.02 m. (6.5 seconds) (M. Y. Chisti, 1989), perhaps suggesting that light fluctuations are a negligible component of the productivity benefits associated with highly mixed reactors.

Modelers and engineers have attempted to predict the fluid mechanics of raceway ponds, and photobioreactors via Computational Fluid Dynamics (CFD) approaches (Ali, Cheema, Yoon, Do, & Park, 2015; Labatut, Ebeling, Bhaskaran, & Timmons, 2015; Pires, Alvim-Ferraz, & Martins, 2017), but modeling of these systems is complex and a series of simplifications are generally required. For example, the conclusions from CFD models applied to investigate velocity and heat transfer are weakened because all studies to date use average velocities as boundary conditions (Sompech et al., 2012; Zhang, Qi, He, Yu, & Ruan, 2017), missing the dynamics of the flow downstream of the paddlewheel. Similarly, turbulence intensity and the impact of the difference in mixing energy inputs in open raceway ponds are not fully understood. Turbulence intensities used in previous CFD applications for open raceway ponds have been documented at 3.84% (Labatut et al., 2015), and at the default values recommended by commercial CFD codes (Drewry et al., 2015; Pires et al., 2017; Zhang et al., 2017), ranging from

158 5-10%. For the case of open channel flow, for instance, experimental turbulence intensities are
159 reported at 2.8% (Nezu & Rodi, 1986). Other previous research studied particle tracking with
160 neutrally buoyant particles in photobioreactors (Fernandes et al., 2017), but ignore the statistical
161 and temporal nature of turbulence modeling. Previous efforts have demonstrated well-mixed
162 conditions in open raceway ponds, but have considered paddlewheel speeds ranging from 15
163 RPM to 28 RPM (Ali et al., 2015) equivalent to mixing energy inputs estimated at 4.5 $W.m^{-3}$ to
164 30 $W.m^{-3}$ or two to 15 times higher than used for industrial cultivation (McGowen et al., 2017;
165 Sompech et al., 2012). None of the reviewed studies have analyzed algae/cyanobacteria cell
166 motion using modern experimental fluid mechanics tools, and CFD tools at industrially relevant
167 mixing energy inputs.
168 Two modern methods for experimental fluid mechanics are particle image velocimetry
169 (PIV) and Acoustic Doppler Velocimetry (ADV). PIV correlates the velocity of the fluid from
170 the distance traveled in a short period of time by neutrally buoyant particles, captured by laser
171 technology and high-resolution cameras (D. Adhikari & E. Longmire, 2012; Foeth, Van Doorne,
172 Van Terwisga, & Wieneke, 2006; Jeon & Sung, 2011; Khalitov & Longmire, 2002; Kiger & Pan,
173 2000). Biological applications include; for instance, aquatic predator-prey interactions (D.
174 Adhikari & E. K. Longmire, 2012), hydrodynamics of fish in aquatic environments (Gemmell,
175 Adhikari, & Longmire, 2014), and fluid transport by plankton aggregations (Wilhelmus &
176 Dabiri, 2014). ADV correlates the velocity of the fluid from the speed of sound of an acoustic
177 pulse (Kraus, Lohrmann, & Cabrera, 1994; Lohrmann, Cabrera, & Kraus, 1994). This technique
178 has been widely used to understand turbulence in natural and engineered civil works including
179 open channels (Blanckaert & Lemmin, 2006; Doroudian, Hurther, & Lemmin, 2007; García,
180 Cantero, Niño, & García, 2007; Hurther & Lemmin, 2001; Nikora & Goring, 1998; Parsheh,

181 Sotiropoulos, & Porté-Agel, 2010; Rusello & Cowen, 2011). A previous study utilized ADV to
182 describe the velocity field of raceway ponds (Chiaramonti et al., 2013), but did not consider the
183 timescales and turbulence conditions of these reactors. In general, there is a poor understanding
184 of the turbulence of flat-panel photobioreactors and open raceway ponds, and the impact of
185 turbulent mixing on the light and dark oscillations experienced by photoautotrophic
186 microorganisms is not conclusive.

187 Based on this understanding of the literature we seek to understand the role of turbulent
188 mixing on the fluid mechanics experienced by photoautotrophic microorganisms during
189 cultivation. Therefore, we conducted (i) pilot-scale fluid mechanics experimentation in open
190 raceway ponds and flat-panel photobioreactors at industrially relevant mixing energy inputs, and
191 (ii) applied computational fluid dynamics modeling and validation. By studying turbulence as a
192 function of mixing energy input in open raceway ponds and flat-panel photobioreactors, we aim
193 to understand the role turbulence plays in the motion of photoautotrophic microorganisms in
194 pilot-scale systems.

195 ## 2. Materials and Methods

196 To evaluate the implications of turbulent mixing on the fluid mechanics experienced by
197 photoautotrophic microorganisms in pilot scale open raceway ponds and flat-panel
198 photobioreactors, we must understand the connections between fluid mechanics and
199 photoautotrophic microorganisms motion under different mixing energy inputs. The workflow,
200 illustrated in Figure 1, integrates parallel but complementary experimental and computational
201 fluid mechanics efforts. By incorporating laboratory experiments at industrially relevant mixing
202 conditions, we can generate comparison and validation between laboratory and industrial scale
203 modeling and experimentation.

204 ## 2.1 Flat-Panel Photobioreactors Configuration

205 To validate the CFD models, we performed experimental work under various mixing
206 energy inputs to the flat-panel photobioreactor. As illustrated in Figure 2, fluid mechanics
207 experimentation was carried out in one replicate of 1L flat-panel photobioreactors made in
208 acrylic with the surface to volume ratio of 112 $m^2 \cdot m^{-3}$. The experiments were at water depths of
209 20 cm. The systems were mixed by sparged air at the bottom of the flat-panel photobioreactors at
210 industrially relevant mixing inputs of 0.7, 0.35, and 0.17 m^3 of air per minute per cubic meter of
211 the reactor, commonly referred as VVM (Quinn et al., 2012). The equivalent mixing energy
212 inputs used in the flat-panel photobioreactors experiments were 1.94, 0.97, and 0.47 $W.m^{-3}$.

213 ## 2.2 Open Raceway Pond Configuration

214 As illustrated in Figure 3, the open raceway pond fluid mechanics experimentation was
215 carried out in one replicate 700L fiber-reinforced plastic raceway at water depths of 20 cm. The
216 system included a paddlewheel provided with a 90V DC Gearmotor with a rated torque of 33 in.-
217 lb, controlled by an IronHorse DC drive to mix the cultures. The mixing energy inputs used in
218 the open raceway pond experiments were 2.1 $W.m^{-3}$ and 0.7 $W.m^{-3}$. We conducted additional
219 experiments at 0.10 $W.m^{-3}$, an order of magnitude lower than reported in the literature for
220 industrial systems (Sompech et al., 2012).

221 ## 2.3 Experimental and Computational Fluid Mechanics Methods

222 To understand the physics of the open raceway ponds and flat-panel photobioreactors we
223 applied a variety of fluid mechanics tools including Particle Image Velocimetry (PIV), Acoustic
224 Doppler Velocimetry (ADV), and CFD.

2.3.1 Flat-panel photobioreactors fluid characterization by PIV

The velocity field of flat-panel photobioreactors was measured in 2-dimensions (x-velocity and y-velocity components) using PIV. We used mixing energy inputs at 0.47 $W.m^{-3}$, 0.97 $W.m^{-3}$, and 1.94 $W.m^{-3}$ in the study of the flat photobioreactor. The study utilized 20 mm PMMA Rhodamine-B particles, Nd:YLF Single Cavity Diode Pumped Solid State High Repetition Rate, laser with 0.2 mm thick measurement plane, double frame CMOS camera, DaVis software for processing 999 samples at 500 hz, and 32x32 double pass followed by a 12x12 single pass interrogation window. Turbulence characterization is described in detail in the next section.

2.3.2 Open raceway pond fluid characterization by ADV

The velocity field in the open raceway pond was measured in 3-dimensions (x-velocity, y-velocity, and z-velocity components) using ADV. We measure fluid velocities at three different cross sections (CS): (i) downstream of the paddlewheel, (ii) at the first turn, and (iii) at the straight channel. At each cross-section, we collected data in a 5X5 matrix with a Vectrino plus firmware + NORTEK. We collected 60,000 ADV samples at 50 Hz at each point. We repeated the experiment at mixing energy inputs of 2.1 $W.m^{-3}$, 0.7 $W.m^{-3}$, and 0.1 $W.m^{-3}$. We describe turbulence by Reynolds decomposition, which includes the steady mean velocity (U) and the fluctuating component ($u'(t)$) from the experimental data (Eq. 1) (Pope & Pope, 2000). The mean fluctuating components in 3-dimensions was used to compute turbulence kinetic energy (k) (Eq. 2) (Pope & Pope, 2000). Lastly, turbulence intensities, defined as the ratio of the velocity fluctuations (u') to the mean velocity (U) were computed from the experimental data (Eq. 3) (Russo & Basse, 2016; Schlichting & Gersten, 2016).

$$u(t) = U + u'(t) \quad \text{Eq. 1}$$

$$k = 1/2 * \left(u'_x{}^2 + u'_y{}^2 + u'_z{}^2\right) \quad \text{Eq. 2}$$

$$I \equiv \frac{u'}{U} \quad \text{Eq. 3}$$

2.3.3 Characterizing cell motion by CFD

To understand the frequency of photoautotrophic microorganism's motion in flat-panel photobioreactors and open raceway ponds, we obtained particle tracks from the CFD models in a Lagrangian representation of the flow. We computed the length and time scales from Kolmogorov microscales (Pope & Pope, 2000; Tennekes & Lumley, 1972; Versteeg & Malalasekera, 2007). The smallest length scales of motion (η) are computed by dimensional analysis as a function of the largest length scale (l) and the Reynolds number (Re) (Eq. 4), and, the smallest time scales (τ) are a function of the largest time scale (T) and the Reynolds number (Eq. 5). The viscous sub-layer in contact with a smooth wall is computed from a linear relationship between the mean velocity (U), wall shear stress (τ_w), viscosity (μ), and the distance from the wall (y) (Eq. 6) (Pope & Pope, 2000; Versteeg & Malalasekera, 2007).

$$\eta = \frac{l}{Re^{3/4}} \quad \text{Eq. 4}$$

$$\tau = \frac{T}{Re^{1/2}} \quad \text{Eq. 5}$$

$$y = \mu \frac{U}{\tau_w} \quad \text{Eq. 6}$$

The characteristic length of the flat-panel photobioreactor and open raceway pond are 0.20 m. and 0.46 m., respectively. The Reynolds number of the flat-panel photobioreactors for mixing energy inputs of 0.03 W.m^{-3}, 0.47 W.m^{-3}, and 0.97 W.m^{-3} are 2.9E^2, 3.6E^2, and 4.1E^2, respectively. For the case of the open raceway pond, the Reynolds number at 0.1 W.m^{-3}, 0.7 W.m^{-3}, and 2.1 W.m^{-3} are 3.5E^4, 6.8E^4, and 9.3E^4, respectively. The wall distance at 0.1 W.m^{-3}, 0.7 W.m^{-3}, and 2.1 W.m^{-3} are 0.0009 m, 0.0005 m , and 0.0002 m, respectively. We designed the

meshes of the flat-panel photobioreactor and open raceway pond at length scales of 0.0008 m. and 0.002 m., respectively, in Trelis 16.3. We developed CFD models in ANSYS Fluent 16.1 for the flat-panel photobioreactor and open raceway pond. The inlet velocity measured from PIV and ADV (Sections 2.3.1 and 2.3.2), and the turbulence intensities, were used as boundary conditions for the flat-panel photobioreactor and open raceway pond. The finite volume method was selected to guarantee conservation of mass, and Direct Numerical Simulation (DNS) was applied (Moin & Mahesh, 1998; Versteeg & Malalasekera, 2007). The time steps used for flat-panel photobioreactors CFD simulations were 0.02 seconds for mixing energy inputs of 0.03 $W.m^{-3}$, 0.47 $W.m^{-3}$, and 0.97 $W.m^{-3}$. We performed CFD simulations for the case of the open raceway pond, at 0.1 $W.m^{-3}$, 0.7 $W.m^{-3}$, and 2.1 $W.m^{-3}$ at time steps of 0.2, 0.1, and 0.05 seconds, respectively. We validated the CFD results against experimental velocity in x-velocity data. This validation was accomplished by comparing the experimental and CFD results as illustrated for the open raceway pond in the Supplementary Material (Figure A5). In figure A5, we represent the height (y) of the reactor normalized to half the water column (H/2) as a function of the normalized velocity, defined as the final velocity normalized to the velocity at half the water column.

To understand the influence of turbulent mixing on the motion of photoautotrophic microorganisms, we computed artificial particle tracks in the flat-panel photobioreactor and open raceway pond by integrating the CFD velocity field (Pope & Pope, 2000). Using particle tracks to model the paths of the cyanobacteria cells in the raceway or photobioreactor assumes that the cells are neutrally buoyant and that inertial forces dominate over gravity and buoyancy forces. From the particle tracks ($x(n)$, $x(n-1)$), we computed the frequency of motion of these particles in the depth or y-axis of the reactors with respect to the moving average of each particle

position. The moving average ($y(n)$) is computed as the mean value by considering an equal number of data points at each side of the central value, known as the sample window (SW) (Eq. 7) (Schafer & Oppenheim, 1989). The sample window for the flat-panel photobioreactor and open raceway pond are 100 and 1000 points. Lastly, the natural frequency (f) is computed as the number of oscillations (n) cyanobacteria cells pass by the top of the chamber, divided by the time length (L_T). The time length of the flat-panel photobioreactors and the open raceway pond are 60 seconds and 15 seconds.. The moving average and frequency were computed from five samples for the flat-panel photobioreactor and open raceway pond.

$$y(n) = \frac{1}{SW} * (x(n) + x(n-1) + \ldots + x(n-(SW-1))) \quad \text{Eq 7}$$

$$f = \frac{n}{L_T} \quad \text{Eq 8}$$

To understand the spectrum and dissipation of eddies as a function of mixing energy inputs in the open raceway ponds, we computed the spectral energy and turbulent dissipation rate (Pope & Pope, 2000; Versteeg & Malalasekera, 2007). The calculation of the spectral energy (ε) can vary in the wavelength as denoted in equations 11 to 13, being a function of viscosity (ν) (Equation 9), turbulence kinetic energy (k), α ~1.5, wavenumber (ω) (Equation 10), characteristic length (l), and the mean velocity (u) (Pope & Pope, 2000; Versteeg & Malalasekera, 2007). The turbulent dissipation rate is a function of c_μ ~ 0.09, k, and l (Pope & Pope, 2000). Spectral energy and turbulent dissipation rate were computed in the open raceway pond at mixing energy inputs 0.1 W.m^{-3}, 0.7 W.m^{-3}, and 2.1 W.m^{-3}.

$$\nu = \mu/\rho \quad \text{Eq 9}$$

$$\omega = 2 * \pi/\eta \quad \text{Eq 10}$$

$$S = \nu^{5/4} * k^{1/4} \qquad For\ \eta \leq 0.001 \quad \text{Eq 11}$$

$$S = \alpha * \omega^{-5/3} * k^{2/3} \quad For\ l \geq \eta \geq 0.001 \quad \text{Eq 12}$$

316 $S = l * u^2 \qquad For\ \eta \geq l$ Eq 13

317 $\varepsilon = {c_\mu}^{3/4} * \frac{k^{3/2}}{l}$ Eq 14

318 ## 3. Results and Discussion

319 We synthesize the results of this research into three aspects. First, we present the flat-panel
320 photobioreactor experimental fluid mechanics results and discuss the motion in these systems.
321 Second, we present the open raceway pond experimental fluid mechanics results and focus the
322 discussion on novel contributions to the field by understanding the turbulence intensities with
323 differences in mixing energy input. Third, we evaluate the impact of differences in mixing
324 energy inputs in the motion of photoautotrophic microorganisms by applying the validated CFD
325 models to both flat-panel photobioreactors and open raceway ponds.

326 ### 3.1 Flat-panel photobioreactor flow characterization

327 The velocity field of the flat-panel photobioreactor at low and high mixing energy inputs are
328 illustrated in Figure 4. The mean velocity computed from PIV at mixing energy inputs of 0.47
329 $W.m^{-3}$, 0.97 $W.m^{-3}$ and 1.94 $W.m^{-3}$ are 0.015 $m.s^{-1}$, 0.018 $m.s^{-1}$, and 0.020 $m.s^{-1}$, respectively.
330 For mixing energy inputs of of 0.47 $W.m^{-3}$, 0.97 $W.m^{-3}$ and 1.94 $W.m^{-3}$ the turbulence intensities
331 are 1.4%, 1.2%, and 1.0%, respectively.Turbulent dissipation for these mixing energy inputs are
332 $1.3E^{-5}$ $m^2.s^{-3}$, $1.7E^{-5}$ $m^2.s^{-3}$, and $1.5E^{-5}$ $m^2.s^{-3}$.

333 These turbulence dissipation rates we obtained are from about four order of magnitudes
334 smaller than those used by Xiao et al. (2016), in their measurements of maximized phosphorous
335 uptake rates and growth decay in different cyanobacteria strains. These results demonstrate the
336 significant differences in the fluid environments maintained under industrially relevant mixing
337 energy inputs relative to laboratory conditions, impacting the biological responses of
338 photoautotrophic microorganisms.

The buoyancy of air bubbles supplied by the air sparger drives the flow circulation in the pilot flat-panel photobioreactors. Buoyancy of an air bubble is a function of bubble size, and the orifice size primarily dictates the bubble sizes on the air sparger. This physics can be analytically described by Stokes Equation (Eq. 15). For small bubbles shaped as spheres due to surface tension, the bubble velocity is a function of gravity (g), bubble diameter (d), dynamic viscosity of liquid (μ), density of liquid (ρ_{Water}), and the density of air bubble ($\rho_{Air\ Bubble}$) (Stokes, 1880; Talaia, 2007). Because bubble buoyancy and therefore bubble velocity is relatively constant at all sparge rates, the velocity of the entrained fluid above the air sparger is relatively constant. The flow circulation in the flat-panel photobioreactors, as a result, is relatively constant over the span of industrially relevant mixing energy inputs studied in our research.

$$Velocity = \frac{1}{18} * g * d^2 \left(\frac{\rho_{Water} - \rho_{Air\ Bubble}}{\mu}\right) \quad \text{Eq. 15}$$

This model explains how the experimentally measured mean velocity of the photobioreactors is relative constant, even under a 4x increase in mixing energy.

3.2 Pilot-scale open raceway pond flow characterization

By applying experimental ADV, we seek to understand turbulence as a function of industrially relevant mixing energy inputs in pilot open raceway ponds. The experimental velocity components (x, y, z) downstream of the raceway paddle wheel are illustrated for the 2.1 $W.m^{-3}$ mixing energy input in Figure 5. The Supplementary Material (Figure A2) illustrates the instantaneous velocity measured at each point in the cross-section. We computed the velocity magnitude, turbulence dissipation rates, and turbulence intensities from these experimental data. Turbulence intensities, downstream from the raceway paddlewheel, are illustrated in Figure 6.

We used these experimental velocities and turbulence intensities as boundary conditions of the CFD models. We computed the velocity field of the fluid domain in the open raceway

362 pond by CFD models at mixing energy inputs 0.1 $W.m^{-3}$, 0.7 $W.m^{-3}$, and 2.1 $W.m^{-3}$ (Figure 7 and
363 Figure A3). Figure 7 illustrates the velocity field of the CFD model at mixing energy inputs of
364 0.1 $W.m^{-3}$. We validated the CFD models against experimental data measured at the 2nd and 3rd
365 cross-section of the open raceway pond, located in the first turn and the straight channel as
366 illustrated in the Supplementary Material (Figure A1 and A5).

367 These results demonstrate that previous studies applying CFD to open raceway ponds
368 have overestimated boundary condition and mean turbulence intensities. At mixing energy inputs
369 of 0.1 $W.m^{-3}$, 0.7 $W.m^{-3}$, and 2.1 $W.m^{-3}$ the velocity magnitudes computed from the experimental
370 ADV data downstream of the raceway paddlewheel are 0.08 $m.s^{-1}$, 0.15 $m.s^{-1}$, and 0.21 $m.s^{-1}$.
371 Turbulence dissipation rates at these industrially relevant mixing energy inputs are $6.1E^{-4}$ m^2/s^{-3},
372 $2.8E^{-3}$ m^2/s^{-3}, and $1.1E^{-2}$ m^2/s^{-3}. For example, turbulence dissipation rates at mixing energy
373 inputs of 0.1 $W.m^{-3}$ and 0.7 $W.m^{-3}$ were found to be three and two order of magnitudes smaller
374 than used by Xiao et al. (2016).

375 Turbulence intensities computed from our experimental work in a pilot open raceway
376 pond at 0.1 $W.m^{-3}$, 0.7 $W.m^{-3}$, and 2.1 $W.m^{-3}$ are 1.02%, 1.05%, and 1.25%, respectively (Figure
377 9.6). We observed low-quality data in the upper left point at a mixing energy input of 0.1 $W.m^{-3}$,
378 with a low signal-to-noise ratio (below ten with no significant implication for the average value
379 calculation). The turbulence intensities used by Labatut et al. (2015) are about three to four times
380 higher than what our research has measured at industrially relevant mixing energy inputs.. The
381 turbulence intensities used by Drewry et al. (2015), Pires et al. (2017), and Zhang et al. (2017)
382 are four to ten times higher than was found in our experimental work. Overestimated turbulence
383 intensities, as a result, can impact the flow dynamics and turbulence in these open raceway
384 ponds, leading to erroneous CFD results. By validating our CFD model with ADV data under

385 different mixing energy inputs, we have found that the results of the CFD models were sensitive
386 to these boundary conditions, including velocity profiles and turbulence intensities. The
387 Supplementary Material (Figure A5) illustrates the validation of the open raceway pond CFD
388 model.

389 ### 3.3 Differences in mixing energy have no significant impact on the frequency of cells motion

390 Finally, we observed that varying mixing energy inputs had no significant effect on the
391 frequency of fluid motion in the flat-panel photobioreactors and open raceway ponds. By
392 conducting experimental and computational fluid mechanics, we have demonstrated that the
393 frequencies of light/dark cycling experienced by photoautotrophic microorganisms cultures in
394 flat-panel photobioreactors and open raceway are not influenced at industrially relevant mixing
395 energy inputs. We have demonstrated this by computing the frequency of this light/dark cycling
396 (Figure 8) from randomly selected particles traveling in the flat-panel photobioreactor and open
397 raceway pond (Figure A4).

398 In the flat-panel photobioreactor, the frequency of motion of the photoautotrophic
399 microorganisms is driven by the buoyancy of air bubbles, in which frequencies of this motion at
400 mixing energy inputs of 0.47 $W.m^{-3}$, 0.97 $W.m^{-3,}$ and 1.94 $W.m^{-3}$ are 0.036 Hz, 0.032 Hz, and
401 0.038 Hz, respectively. By performing a one-way analysis of variance (ANOVA), we conclude
402 that differences in mixing energy inputs have no significant impact on the frequencies of fluid
403 motion (and therefore organism light exposure), as illustrated in Figure 8. The frequencies of
404 flashing lights used by Janssen, Tramper, Mur, & Wijffels (2003) and Vejrazka, Janssen,
405 Streefland, & Wijffels (2011, 2012) are from about 13 to 300 times higher than observed in our
406 experimental work at industrially relevant mixing energy inputs. Our frequencies of motion are
407 consistent with the frequencies studied by Grobbelaar (1991) and the frequencies estimated for

408 fermenters by M. Y. Chisti (1989). Our results demonstrate that the buoyancy of air bubbles
409 drives flow circulation in flat-panel photobioreactors, maintaining a relatively constant
410 circulation in the reactor regardless of variation in mixing energy input.

411 In the pilot open raceway pond, the frequency of motion of the photoautotrophic
412 microorganisms is not significantly impacted by changes in industrially relevant mixing energy
413 inputs. Frequencies of motion at mixing energy inputs of 0.1 $W.m^{-3}$, 0.7 $W.m^{-3}$, and 2.1 $W.m^{-3}$
414 are 0.272 Hz, 0.364 Hz, and 0.358 Hz. By performing a one-way ANOVA of these frequencies,
415 we found no significant impact due to differences in mixing energy input (Figure 8). Similar to
416 the results for the photobioreactors, the frequencies of flashing lights used by Janssen, Tramper,
417 Mur, & Wijffels (2003) and Vejrazka, Janssen, Streefland, & Wijffels (2011, 2012) are from
418 about 1 to 40 order of magnitudes higher than observed in our experimental work at industrially
419 relevant mixing energy inputs. Our frequencies of motion are consistent with the frequencies
420 estimated for airlift reactors by M. Y. Chisti (1989). Since the light/dark cycling frequencies
421 experienced by the photoautotrophic cells are not significantly impacted by mixing energy input,
422 our research suggests that well-mixed conditions exist at the mixing energy levels used in
423 industrial open raceway ponds, and that increased mixing rates do not improve cultivation
424 productivity by changing the light regime of the culture.

425 The spectral energy computed for mixing energy inputs in a pilot open raceway pond at
426 0.1 $W.m^{-3}$, 0.7 $W.m^{-3}$, and 2.1 $W.m^{-3}$ (Figure 9) follows the vortex stretching process described
427 in the turbulence literature including Pope & Pope (2000) and Versteeg & Malalasekera (2007).
428 In this process, the largest eddies extract energy from the mean velocity, eddies are stretched as
429 one end moves faster than the other end, and angular momentum is conserved as eddies are
430 dissipated. Therefore, as eddies dissipate, the rotation of eddies increase and cross-section radius

431 of eddies decrease. Dissipation of energy occurs faster at higher mixing energy inputs, 0.7 $W.m^{-3}$
432 and 2.1 $W.m^{-3}$ as illustrated in figure 9, where turbulence kinetic energy and turbulent dissipation
433 rate are higher. The characteristic length (L) is theoretically constant regardless of mixing energy
434 input, as it is theoretically a function of the open channel height (H) and width (W) of the open
435 raceway pond (Eq. 16). The convective time scales, however, are reduced with increased mixing
436 energy because increases in the input velocity magnitude (U) increases the frequency of largest
437 eddies in the system (Eq. 17). Although input velocity magnitudes at high mixing energy inputs
438 (2.1 $W.m^{-3}$) are about three times higher than at low mixing energy inputs (0.1 $W.m^{-3}$), kinetic
439 energy is dissipated about 18 times faster at mixing energy inputs of 2.1 $W.m^{-3}$ as illustrated in
440 the experimental turbulence dissipation rates in section 3.2 and in the Supplementary Material
441 (Figure A6). This analysis suggests that despite the increase of largest eddy frequency (Figure 9)
442 at high mixing energy inputs, turbulence dissipation decreases the frequency of cell motion in
443 open raceway ponds (Figure 8).

444 $$L = \frac{4*H*W}{2*H+W} \quad \text{Eq. 16}$$

445 $$Convective\ Time\ Scales = \frac{L}{U} \quad \text{Eq. 17}$$

446 These results demonstrate that differences in mixing energy input have no significant impact
447 on the overall light/dark cycling frequecies experienced by photoautotrophic cells in pilot flat-
448 panel photobioreactors and open raceway ponds. These results provide evidence to disprove the
449 hypothesis that light regime experienced by photoautotrophic organisms influences their
450 productivity, over the range of industrially relevant mixing energies and mechanisms considered
451 here. Alternative hypotheses, describing the effects of mixing energy input on the thermal,
452 chemical, and biological response of these organisms is not addressed in this research.

4. Conclusions

A combination of experimental and computational fluid mechanics measurements has been used to quantify the mixing conditions in pilot flat-panel photobioreactors and open raceway ponds. Our experimental and computational work has demonstrated that differences in mixing energy do not have a significant impact on the frequency of microorganisms' motion within the cultviation systems, and therefore do not influence the light/dark dynamics of the light regime experienced during cultivation. These measurements provide new boundary condition measurements as inputs for photobioreactor and raceway pond CFD practitioners, and demonstrate CFD results validated using a variety of experimental techniques.

Acknowledgments

The authors acknowledge the National Science Foundation grant number 1332404. Additionally, the authors acknowledge Dr. Xinfeng Gao, Mechanical Engineering Department of Colorado State University; for providing valuable feedback concerning computational fluid dynamic modeling. Dr. Chris Thornton and Natalie Youngblood, Department of Civil Engineering of Colorado State University, for facilitating the ADV device and protocols used in this research. The graduate and undergraduate students of the Mechanical Engineering Department of Colorado State University that participated in the Research Experience and Mentoring (REM) program funded by National Science Foundation; Pengyu Cao, Alex Jones, Kevin Bennett, Matthew Knopf, and Chase Fogus. Sandia National Laboratories is a multimission laboratory managed and operated by National Technology & Engineering Solutions of Sandia, LLC, a wholly owned subsidiary of Honeywell International Inc., for the U.S. Department of Energy's National Nuclear Security Administration under contract DE-

475 NA0003525. The views expressed in the article do not necessarily represent the views of the
476 U.S. Department of Energy or the United States Government.

477

478 ## References

479 Adhikari, D., & Longmire, E. (2012). Visual hull method for tomographic PIV measurement of
480 flow around moving objects. *Experiments in fluids, 53*(4), 943-964.

481 Adhikari, D., & Longmire, E. K. (2012). Infrared tomographic PIV and 3D motion tracking
482 system applied to aquatic predator–prey interaction. *Measurement Science and Technology,*
483 *24*(2), 024011.

484 Al□Rubeai, M., Singh, R., Goldman, M., & Emery, A. (1995). Death mechanisms of animal
485 cells in conditions of intensive agitation. *Biotechnology and bioengineering, 45*(6), 463-472.

486 Ali, H., Cheema, T. A., Yoon, H. S., Do, Y., & Park, C. W. (2015). Numerical prediction of
487 algae cell mixing feature in raceway ponds using particle tracing methods. *Biotechnology and*
488 *bioengineering, 112*(2), 297-307.

489 Barbosa, M. J., & Wijffels, R. H. (2004). Overcoming shear stress of microalgae cultures in
490 sparged photobioreactors. *Biotechnology and bioengineering, 85*(1), 78-85.

491 Blanckaert, K., & Lemmin, U. (2006). Means of noise reduction in acoustic turbulence
492 measurements. *Journal of hydraulic Research, 44*(1), 3-17.

493 Brune, D., Lundquist, T., & Benemann, J. (2009). Microalgal biomass for greenhouse gas
494 reductions: potential for replacement of fossil fuels and animal feeds. *Journal of Environmental*
495 *Engineering, 135*(11), 1136-1144.

496 Chalmers, J. J. (2015). Mixing, aeration and cell damage, 30+ years later: what we learned, how
497 it affected the cell culture industry and what we would like to know more about. *Current*
498 *Opinion in Chemical Engineering, 10*, 94-102.

499 Chiaramonti, D., Prussi, M., Casini, D., Tredici, M. R., Rodolfi, L., Bassi, N., . . . Bondioli, P.
500 (2013). Review of energy balance in raceway ponds for microalgae cultivation: Re-thinking a
501 traditional system is possible. *Applied energy, 102*(Supplement C), 101-111.
502 doi:https://doi.org/10.1016/j.apenergy.2012.07.040

503 Chisti, M. Y. (1989). *Airlift bioreactors*: Elsevier Applied Science.

504 Chisti, Y. (2007). Biodiesel from microalgae. *Biotechnology Advances, 25*(3), 294-306.
505 doi:http://dx.doi.org/10.1016/j.biotechadv.2007.02.001

506 Doroudian, B., Hurther, D., & Lemmin, U. (2007). Discussion of "turbulence measurements with
507 acoustic doppler velocimeters" by Carlos M. García, Mariano I. Cantero, Yarko Niño, and
508 Marcelo H. García. *Journal of Hydraulic Engineering, 133*(11), 1286-1289.

509 Drewry, J. L., Choi, C. Y., An, L., & Gharagozloo, P. E. (2015). A computational fluid dynamics
510 model of algal growth: development and validation. *Transactions of the ASABE, 58*(2), 203-213.

511 Edmundson, S. J., & Huesemann, M. H. (2015). The dark side of algae cultivation:
512 Characterizing night biomass loss in three photosynthetic algae, Chlorella sorokiniana,
513 Nannochloropsis salina and Picochlorum sp. *Algal Research, 12*, 470-476.

514 Fadlallah, H., Jarrahi, M., Herbert, E., Ferrari, R., Mejean, A., & Peerhossaini, H. (2016). *Effects*
515 *of Shear Stress on the Growth Rate of Micro-Organisms in Agitated Reactors.* Paper presented at

516 the ASME 2016 Fluids Engineering Division Summer Meeting collocated with the ASME 2016
517 Heat Transfer Summer Conference and the ASME 2016 14th International Conference on
518 Nanochannels, Microchannels, and Minichannels.

519 Fernandes, B. D., Mota, A., Geada, P., Oliveira, J. L., Teixeira, J. A., Vasconcelos, V., &
520 Vicente, A. A. (2017). Development of a novel user-friendly platform to couple light regime
521 characterization with particle tracking - cells' light history determination during phototrophic
522 cultivations. *Algal Research, 24*(Part A), 276-283.
523 doi:https://doi.org/10.1016/j.algal.2017.04.017

524 Foeth, E., Van Doorne, C., Van Terwisga, T., & Wieneke, B. (2006). Time resolved PIV and
525 flow visualization of 3D sheet cavitation. *Experiments in fluids, 40*(4), 503-513.

526 García, C. M., Cantero, M. I., Niño, Y., & García, M. H. (2007). Closure to "Turbulence
527 Measurements with Acoustic Doppler Velocimeters" by Carlos M. García, Mariano I. Cantero,
528 Yarko Niño, and Marcelo H. García. *Journal of Hydraulic Engineering, 133*(11), 1289-1292.

529 Gemmell, B. J., Adhikari, D., & Longmire, E. K. (2014). Volumetric quantification of fluid flow
530 reveals fish's use of hydrodynamic stealth to capture evasive prey. *Journal of The Royal Society*
531 *Interface, 11*(90), 20130880.

532 Gharagozloo, P. E., Drewry, J. L., Collins, A. M., Dempster, T. A., Choi, C. Y., & James, S. C.
533 (2014). Analysis and modeling of Nannochloropsis growth in lab, greenhouse, and raceway
534 experiments. *Journal of applied phycology, 26*(6), 2303-2314.

535 Grobbelaar, J. U. (1991). The influence of light/dark cycles in mixed algal cultures on their
536 productivity. *Bioresour Technol, 38*(2-3), 189-194.

Han, R. B., & Yuan, Y. J. (2004). Oxidative Burst in Suspension Culture of Taxus cuspidataInduced by a Laminar Shear Stress in Short□Term. *Biotechnology progress, 20*(2), 507-513.

Havens, K. E., James, R. T., East, T. L., & Smith, V. H. (2003). N: P ratios, light limitation, and cyanobacterial dominance in a subtropical lake impacted by non-point source nutrient pollution. *Environmental Pollution, 122*(3), 379-390.

Hurther, D., & Lemmin, U. (2001). A correction method for turbulence measurements with a 3D acoustic Doppler velocity profiler. *Journal of Atmospheric and Oceanic Technology, 18*(3), 446-458.

Janssen, M., Tramper, J., Mur, L. R., & Wijffels, R. H. (2003). Enclosed outdoor photobioreactors: Light regime, photosynthetic efficiency, scale□up, and future prospects. *Biotechnology and bioengineering, 81*(2), 193-210.

Jeon, Y. J., & Sung, H. J. (2011). PIV measurement of flow around an arbitrarily moving body. *Experiments in fluids, 50*(4), 787-798.

Jones, S. M. J., Louw, T. M., & Harrison, S. T. L. (2017). Energy consumption due to mixing and mass transfer in a wave photobioreactor. *Algal Research, 24*(Part A), 317-324. doi:https://doi.org/10.1016/j.algal.2017.03.001

Keane, J. T., Ryan, D., & Gray, P. P. (2003). Effect of shear stress on expression of a recombinant protein by Chinese hamster ovary cells. *Biotechnology and bioengineering, 81*(2), 211-220.

557 Khalitov, D., & Longmire, E. (2002). Simultaneous two-phase PIV by two-parameter phase
558 discrimination. *Experiments in fluids, 32*(2), 252-268.

559 Kiger, K., & Pan, C. (2000). PIV technique for the simultaneous measurement of dilute two-
560 phase flows. *Journal of fluids engineering, 122*(4), 811-818.

561 Kim, H. W., Vannela, R., Zhou, C., Harto, C., & Rittmann, B. E. (2010). Photoautotrophic
562 nutrient utilization and limitation during semi-continuous growth of Synechocystis sp. PCC6803.
563 *Biotechnology and bioengineering, 106*(4), 553-563. doi:10.1002/bit.22724

564 Kim, H. W., Vannela, R., Zhou, C., & Rittmann, B. E. (2011). Nutrient acquisition and limitation
565 for the photoautotrophic growth of Synechocystis sp. PCC6803 as a renewable biomass source.
566 *Biotechnology and bioengineering, 108*(2), 277-285. doi:10.1002/bit.22928

567 Kraus, N. C., Lohrmann, A., & Cabrera, R. (1994). New acoustic meter for measuring 3D
568 laboratory flows. *Journal of Hydraulic Engineering, 120*(3), 406-412.

569 Kumar, K., Dasgupta, C. N., Nayak, B., Lindblad, P., & Das, D. (2011). Development of suitable
570 photobioreactors for CO 2 sequestration addressing global warming using green algae and
571 cyanobacteria. *Bioresource technology, 102*(8), 4945-4953.

572 Kunnen, S. J., Malas, T. B., Semeins, C. M., Bakker, A. D., & Peters, D. J. (2017).
573 Comprehensive transcriptome analysis of fluid shear stress altered gene expression in renal
574 epithelial cells. *Journal of cellular physiology*.

575 Labatut, R. A., Ebeling, J. M., Bhaskaran, R., & Timmons, M. B. (2015). Modeling
576 hydrodynamics and path/residence time of aquaculture-like particles in a mixed-cell raceway

(MCR) using 3D computational fluid dynamics (CFD). *Aquacultural Engineering, 67*(Supplement C), 39-52. doi:https://doi.org/10.1016/j.aquaeng.2015.05.006

Lardon, L., Helias, A., Sialve, B., Steyer, J.-P., & Bernard, O. (2009). Life-cycle assessment of biodiesel production from microalgae. *Environmental science & technology, 43*(17), 6475-6481.

Little, A. (1953). Pilot plant studies in the production of Chlorella. *Algal Culture: From Laboratory to Pilot Plant*, 235-273.

Lohrmann, A., Cabrera, R., & Kraus, N. C. (1994). *Acoustic-Doppler velocimeter (ADV) for laboratory use.* Paper presented at the Fundamentals and advancements in hydraulic measurements and experimentation.

McGowen, J., Knoshaug, E. P., Laurens, L. M., Dempster, T. A., Pienkos, P. T., Wolfrum, E., & Harmon, V. L. (2017). The Algae Testbed Public-Private Partnership (ATP3) framework; establishment of a national network of testbed sites to support sustainable algae production. *Algal Research, 25*, 168-177.

Michels, M. H., van der Goot, A. J., Norsker, N.-H., & Wijffels, R. H. (2010). Effects of shear stress on the microalgae Chaetoceros muelleri. *Bioprocess and biosystems engineering, 33*(8), 921-927.

Microalgal Biotechnology: Potential and Production. (2013). C. Posten & C. Walter (Eds.),

Mirón, A. S., Garcıa, M. C. C., Gómez, A. C., Camacho, F. G., Grima, E. M., & Chisti, Y. (2003). Shear stress tolerance and biochemical characterization of Phaeodactylum tricornutum in

quasi steady-state continuous culture in outdoor photobioreactors. *Biochemical Engineering Journal, 16*(3), 287-297.

Moin, P., & Mahesh, K. (1998). Direct numerical simulation: a tool in turbulence research. *Annual review of fluid mechanics, 30*(1), 539-578.

Moisander, P. H., Hench, J. L., Kononen, K., & Paerl, H. W. (2002). Small□scale shear effects on heterocystous cyanobacteria. *Limnology and Oceanography, 47*(1), 108-119.

Nezu, I., & Rodi, W. (1986). Open-channel flow measurements with a laser Doppler anemometer. *Journal of Hydraulic Engineering, 112*(5), 335-355.

Nguyen, M. A., & Hoang, A. L. (2016). *A review on microalgae and cyanobacteria in biofuel production.* USTH.

Nikora, V. I., & Goring, D. G. (1998). ADV measurements of turbulence: Can we improve their interpretation? *Journal of Hydraulic Engineering, 124*(6), 630-634.

Oswald, W. J. (1988). Large-scale algal culture systems (engineering aspects). *Micro-algal biotechnology. Cambridge University Press, Cambridge*, 357-394.

Parsheh, M., Sotiropoulos, F., & Porté-Agel, F. (2010). Estimation of power spectra of acoustic-Doppler velocimetry data contaminated with intermittent spikes. *Journal of Hydraulic Engineering, 136*(6), 368-378.

Pires, J. C. M., Alvim-Ferraz, M. C. M., & Martins, F. G. (2017). Photobioreactor design for microalgae production through computational fluid dynamics: A review. *Renewable and*

615 *Sustainable Energy Reviews, 79*(Supplement C), 248-254.
616 doi:https://doi.org/10.1016/j.rser.2017.05.064

617 Pope, S. B., & Pope, S. B. (2000). *Turbulent flows*: Cambridge university press.

618 Quinn, J. C., Turner, C. W., & Bradley, T. H. (2012). Scale-Up of flat plate photobioreactors
619 considering diffuse and direct light characteristics. *Biotechnol Bioeng, 109*(2), 363-370.
620 doi:10.1002/bit.23324

621 Rawat, I., Kumar, R. R., Mutanda, T., & Bux, F. (2013). Biodiesel from microalgae: a critical
622 evaluation from laboratory to large scale production. *Applied energy, 103*, 444-467.

623 Richardson, G. M., Lannigan, J., & Macara, I. G. (2015). Does FACS perturb gene expression?
624 *Cytometry Part A, 87*(2), 166-175.

625 Robertson, D., Jacobson, S., Morgan, F., Berry, D., Church, G., & Afeyan, N. (2011). A new
626 dawn for industrial photosynthesis. *Photosynthesis Research, 107*(3), 269-277.
627 doi:10.1007/s11120-011-9631-7

628 Rodolfi, L., Chini Zittelli, G., Bassi, N., Padovani, G., Biondi, N., Bonini, G., & Tredici, M. R.
629 (2009). Microalgae for oil: Strain selection, induction of lipid synthesis and outdoor mass
630 cultivation in a low□cost photobioreactor. *Biotechnology and bioengineering, 102*(1), 100-112.

631 Rusello, P. J., & Cowen, E. A. (2011). *Turbulent dissipation estimates from pulse coherent*
632 *doppler instruments.* Paper presented at the Current, Waves and Turbulence Measurements
633 (CWTM), 2011 IEEE/OES 10th.

634 Russo, F., & Basse, N. T. (2016). Scaling of turbulence intensity for low-speed flow in smooth
635 pipes. *Flow Measurement and Instrumentation, 52*, 101-114.

636 Sánchez Mirón, A., Garcia Camacho, F., Contreras Gomez, A., Grima, E. M., & Chisti, Y.
637 (2000). Bubble□column and airlift photobioreactors for algal culture. *AIChE Journal, 46*(9),
638 1872-1887.

639 Schafer, R. W., & Oppenheim, A. V. (1989). *Discrete-time signal processing*: Prentice Hall
640 Englewood Cliffs, NJ.

641 Schlichting, H., & Gersten, K. (2016). *Boundary-layer theory*: Springer.

642 Sieck, J. B., Budach, W. E., Suemeghy, Z., Leist, C., Villiger, T. K., Morbidelli, M., & Soos, M.
643 (2014). Adaptation for survival: Phenotype and transcriptome response of CHO cells to elevated
644 stress induced by agitation and sparging. *Journal of biotechnology, 189*, 94-103.

645 Sieck, J. B., Cordes, T., Budach, W. E., Rhiel, M. H., Suemeghy, Z., Leist, C., . . . Soos, M.
646 (2013). Development of a scale-down model of hydrodynamic stress to study the performance of
647 an industrial CHO cell line under simulated production scale bioreactor conditions. *Journal of*
648 *biotechnology, 164*(1), 41-49.

649 Sompech, K., Chisti, Y., & Srinophakun, T. (2012). Design of raceway ponds for producing
650 microalgae. *Biofuels, 3*(4), 387-397. doi:10.4155/bfs.12.39

651 Stokes, G. G. (1880). Mathematical and Physical Papers, 1. *Cambridge University Press*.

652 Talaia, M. A. (2007). Terminal velocity of a bubble rise in a liquid column. *World Academy of*
653 *Science, Engineering and Technology, 28*, 264-268.

654 Tennekes, H., & Lumley, J. L. (1972). *A first course in turbulence*: MIT press.

655 Vejrazka, C., Janssen, M., Streefland, M., & Wijffels, R. H. (2011). Photosynthetic efficiency of
656 Chlamydomonas reinhardtii in flashing light. *Biotechnology and bioengineering, 108*(12), 2905-
657 2913.

658 Vejrazka, C., Janssen, M., Streefland, M., & Wijffels, R. H. (2012). Photosynthetic efficiency of
659 Chlamydomonas reinhardtii in attenuated, flashing light. *Biotechnology and bioengineering,*
660 *109*(10), 2567-2574.

661 Versteeg, H. K., & Malalasekera, W. (2007). *An introduction to computational fluid dynamics:*
662 *the finite volume method*: Pearson Education.

663 Wang, J., Lü, D., Mao, D., & Long, M. (2014). Mechanomics: an emerging field between
664 biology and biomechanics. *Protein & cell, 5*(7), 518-531.

665 Weyer, K. M., Bush, D. R., Darzins, A., & Willson, B. D. (2010). Theoretical maximum algal oil
666 production. *Bioenergy Research, 3*(2), 204-213.

667 Wijffels, R. H., Kruse, O., & Hellingwerf, K. J. (2013). Potential of industrial biotechnology
668 with cyanobacteria and eukaryotic microalgae. *Current opinion in biotechnology, 24*(3), 405-
669 413.

670 Wilhelmus, M. M., & Dabiri, J. O. (2014). Observations of large-scale fluid transport by laser-
671 guided plankton aggregations. *Physics of Fluids, 26*(10), 101302.

672 Xiao, Y., Li, Z., Li, C., Zhang, Z., & Guo, J. (2016). Effect of Small-Scale Turbulence on the
673 Physiology and Morphology of Two Bloom-Forming Cyanobacteria. *PloS one, 11*(12),
674 e0168925.

675 Yi, W., Sun, Y., Wei, X., Gu, C., Dong, X., Kang, X., . . . Dou, K. (2010). Proteomic profiling of
676 human bone marrow mesenchymal stem cells under shear stress. *Molecular and cellular*
677 *biochemistry, 341*(1-2), 9-16.

678 Zhang, J.-Y., Qi, H., He, Z.-Z., Yu, X.-Y., & Ruan, L.-M. (2017). Investigation of light transfer
679 procedure and photobiological hydrogen production of microalgae in photobioreactors at
680 different locations of China. *International Journal of Hydrogen Energy, 42*(31), 19709-19722.
681 doi:https://doi.org/10.1016/j.ijhydene.2017.06.079

682
683
684
685
686
687
688
689
690
691
692
693

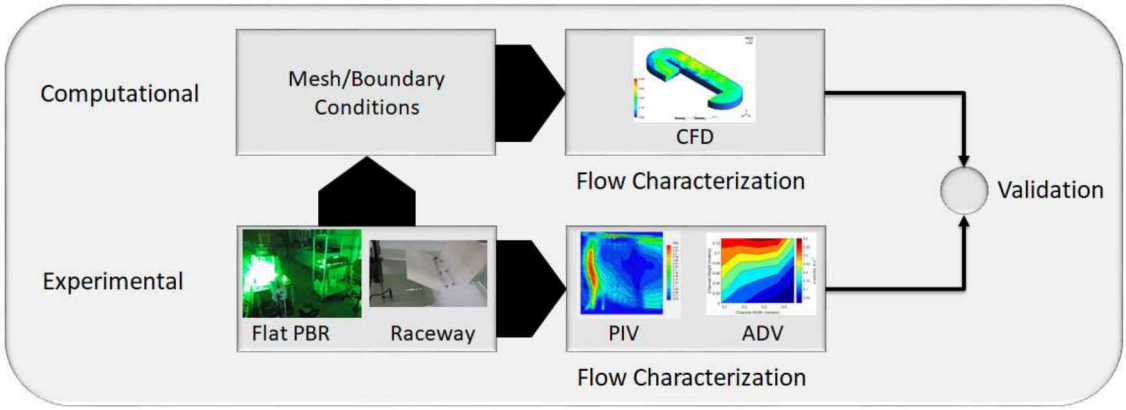

Figure 1. Workflow for experimental and computational fluid mechanics (top flow) and photoautotrophic growth (bottom flow) to assess the impact of mixing energy inputs.

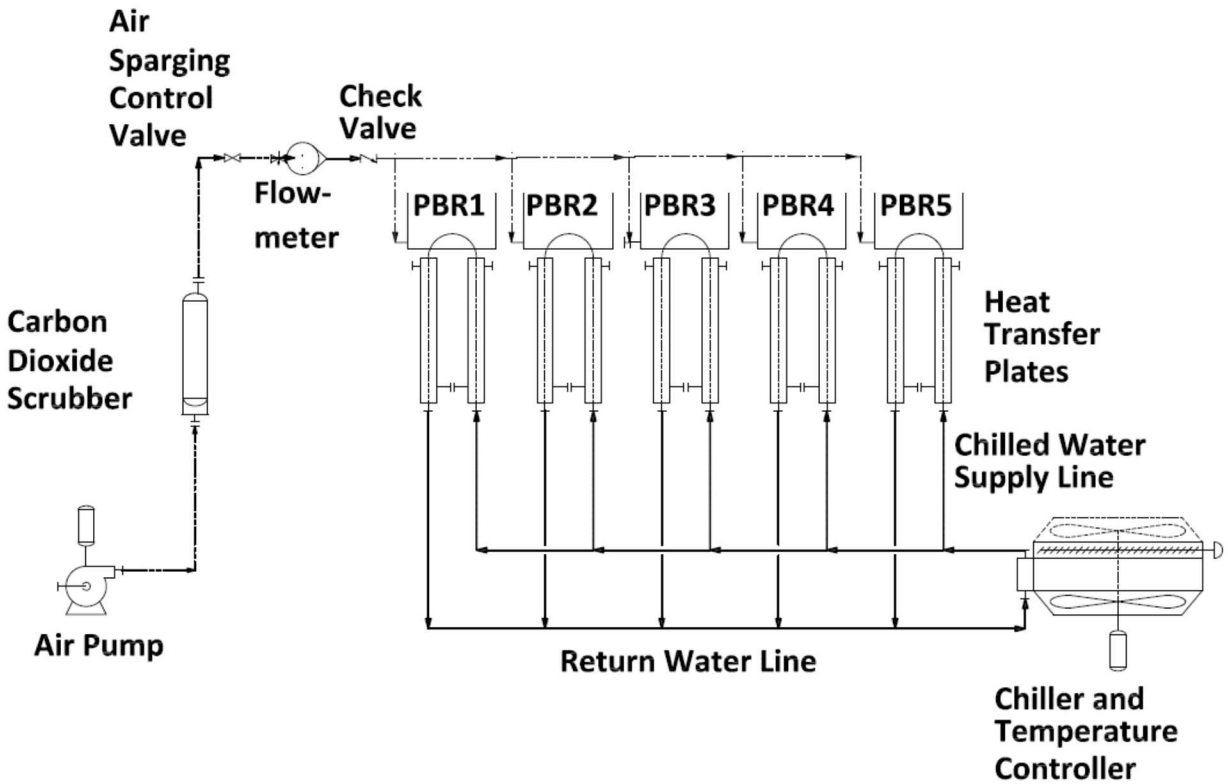

Figure 2. Instrumentation Diagram of Flat-panel photobioreactors system for experimental and model-based analysis.

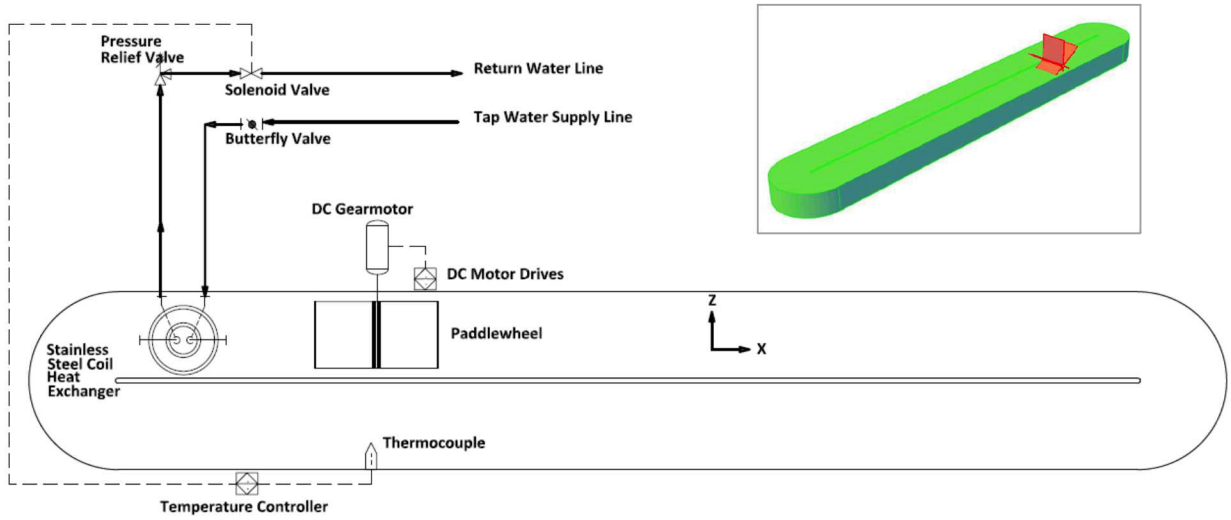

Figure 3. Plan View and Instrumentation Diagram of Open raceway pond system for industrial scale experimental and model-based analysis. The 3D view in the upper right corner illustrates the Open Raceway Pond.

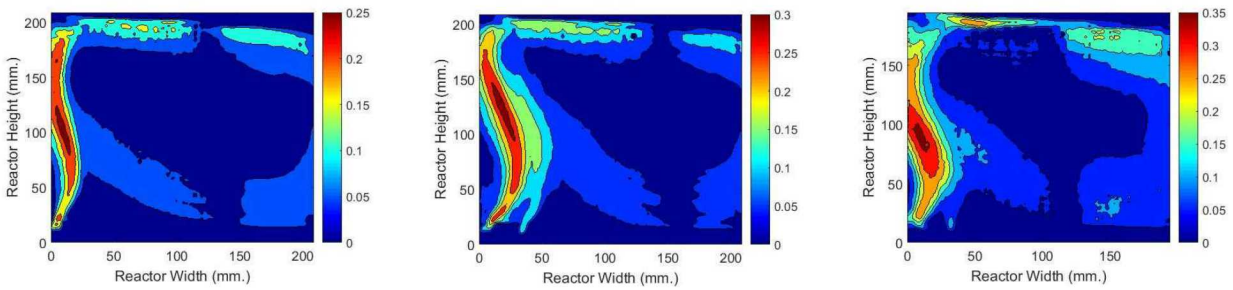

Figure 4. Velocity field ($m.s^{-1}$) obtained from PIV of flat-panel photobioreactor at mixing energy inputs of 0.47 $W.m^{-3}$ (left figure), 0.97 $W.m^{-3}$ (middle figure), and 1.94 $W.m^{-3}$ (right figure).

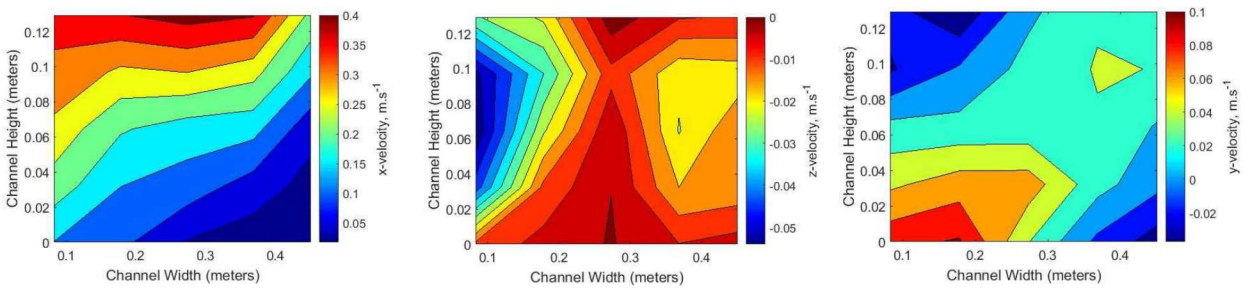

Figure 5. First cross section (downstream paddlewheel) velocity components ($m.s^{-1}$) of open raceway pond at mixing energy input of 2.1 $W.m^{-3}$. The left figure corresponds to the x-velocity, the middle figure corresponds to the y-velocity, and the right figure corresponds to the z-velocity.

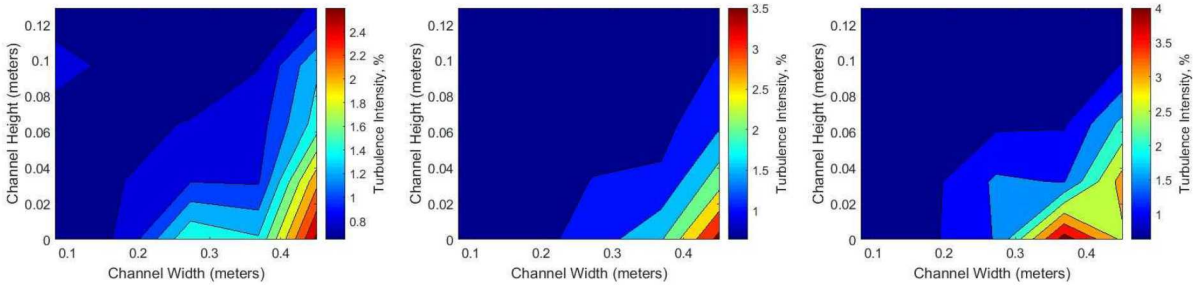

Figure 6. Turbulence intensities (%) of first cross section of open raceway pond at mixing energy inputs of 0.1 $W.m^{-3}$ (left figure), 0.7 $W.m^{-3}$ (middle figure) and 1.94 $W.m^{-3}$ (right figure).

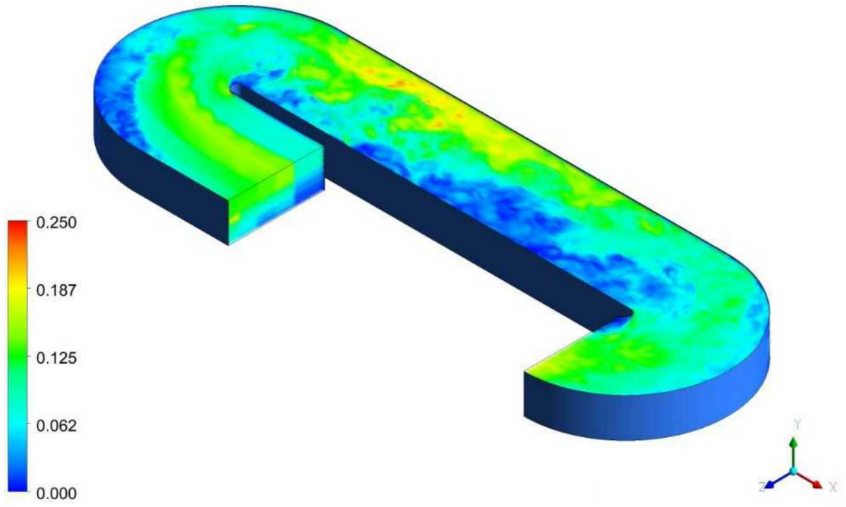

Figure 7. Velocify field (m.s^{-1}) from Direct Numerical Simulation-based CFD model of open raceway pond at mixing energy inputs of 0.1 W.m^{-3}.

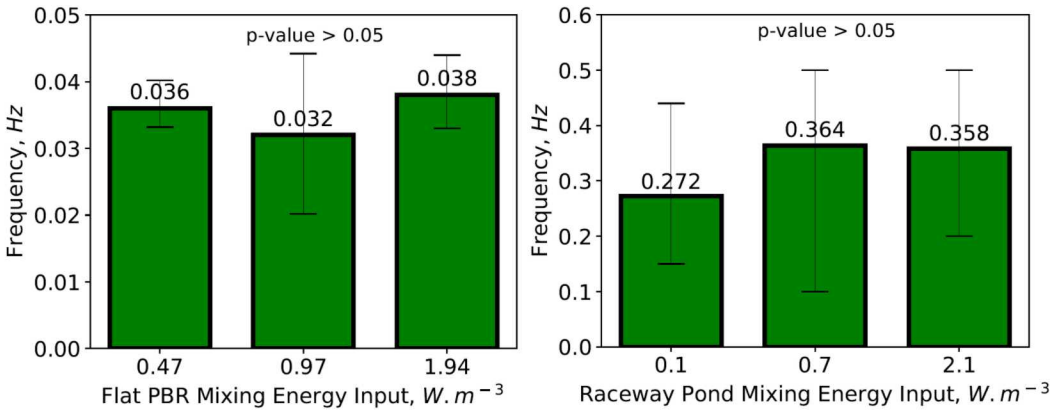

Figure 8. The frequency of photoautotrophic microorganism cell motion in flat-panel photobioreactor (left figure) and open raceway pond (right figure).

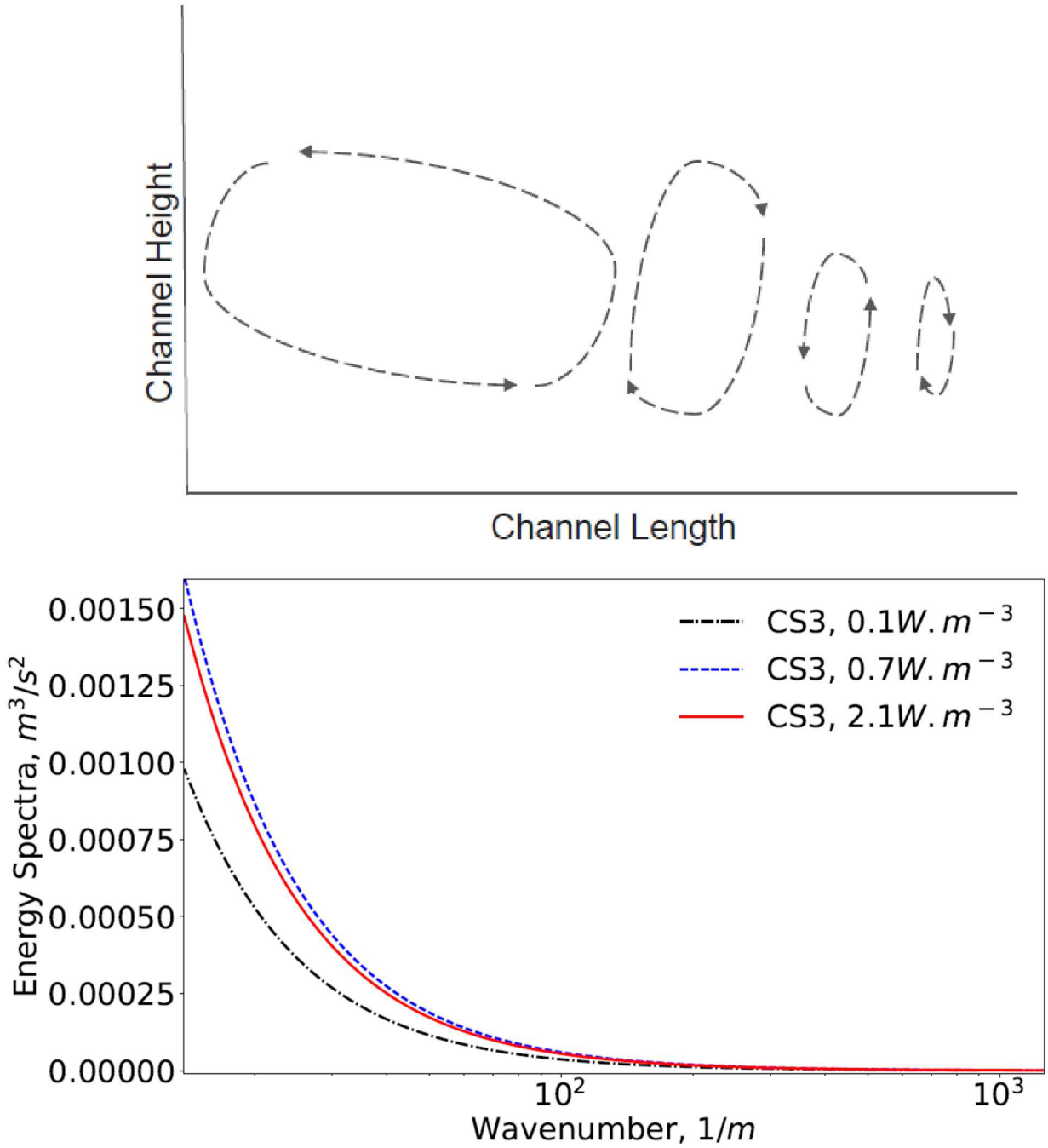

Figure 9. Energy Spectra at the straight channel (CS3) in open raceway pond at mixing energy inputs of 0.1 W.m^{-3}, 0.7 W.m^{-3}, and 1.94 W.m^{-3} computed from experimental ADV data.

Supplementary Material: Pilot-scale open raceway ponds and flat-panel photobioreactors maintain well-mixed conditions under a wide range of mixing energy inputs

Carlos Quiroz-Arita[1], Myra L. Blaylock[2], Patricia E. Gharagozloo[3], David Bark[1], Lakshmi Prasad Dasi[4], Thomas H. Bradley[1]

[1]Mechanical Engineering, Colorado State University, Fort Collins, CO 80524, USA

[2]Sandia National Laboratories, Livermore, CA 94551, USA

[3] Lawrence Livermore National Laboratory, Livermore, CA 94550, USA

[4]Department of Biomedical Engineering, The Ohio State University, Columbus, OH 43210, USA

1. Experimental and Computational Fluid Dynamics of Open Raceway Pond

To understand the frequency of photoautotrophic microorganism's motion in flat-panel photobioreactors and open raceway ponds, we obtained particle tracks from the CFD models in a Lagrangian representation of the flow. The finite volume method was selected to guarantee the conservation of mass, and Direct Numerical Simulation (DNS) was applied to obtain precise details of turbulence (Moin & Mahesh, 1998; Versteeg & Malalasekera, 2007), influencing the motion of photoautotrophic microorganisms. We computed the velocity field of the fluid domain in the open raceway pond by CFD models at mixing energy inputs 0.1 $W.m^{-3}$, 0.7 $W.m^{-3}$, and 2.1 $W.m^{-3}$ (Figure 7 and Figure A3). Figure 7 illustrates the velocity field of the CFD model at mixing energy inputs of 0.1 $W.m^{-3}$. We validated the CFD models against experimental data

measured at the second and third cross-section of the open raceway pond, located in the first turn and the straight channel as illustrated in the Supplementary material (Figure A1 and A5). By integrating experimental and computational fluid mechanics, we have represented the physics in pilot scale environments, demonstrating the fluid dynamics in flat-panel photobioreactors and open raceway ponds do not influence the overall light experienced by photoautotrophic microorganisms cultures. We have demonstrated this by computing the frequency of this motion (Figure 8) from randomly selected particles traveling in the flat-panel photobioreactor and open raceway pond (Figure A4).

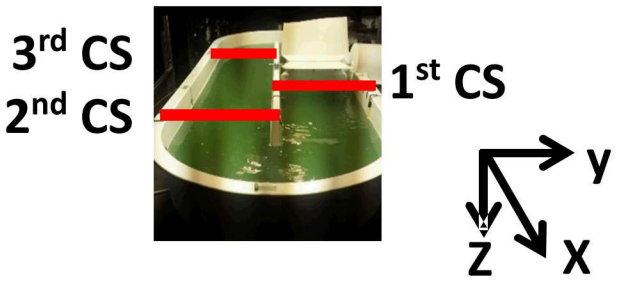

Figure A1. Open raceway pond Coordinates. The x-velocity follows the flow direction downstream the paddlewheel. The y-velocity points toward the vertical wall of the raceway pond. The z-velocity point towards the bottom of the raceway pond. The first cross-section (CS) is located downstream of the paddlewheel. The second CS is located on the first turn of the channel. The third CS is located in the straight channel behind the paddlewheel.

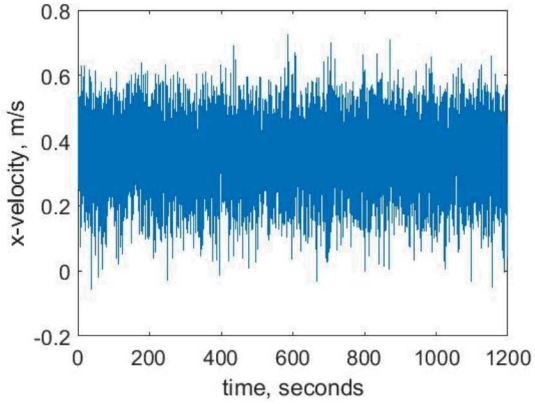

Figure A2. Example of instantaneous velocity measured in open raceway pond by ADV.

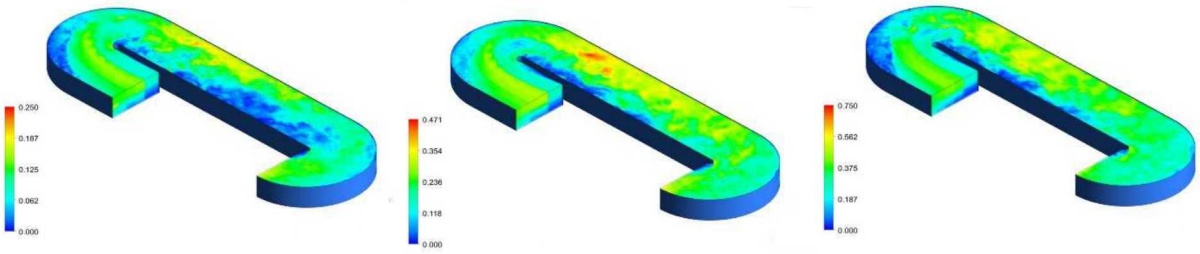

Figure A3. DNS based CFD model of open raceway pond at mixing energy inputs of 0.1 $W.m^{-3}$ (left figure), 0.7 $W.m^{-3}$ (middle figure) and 1.94 $W.m^{-3}$ (right figure).

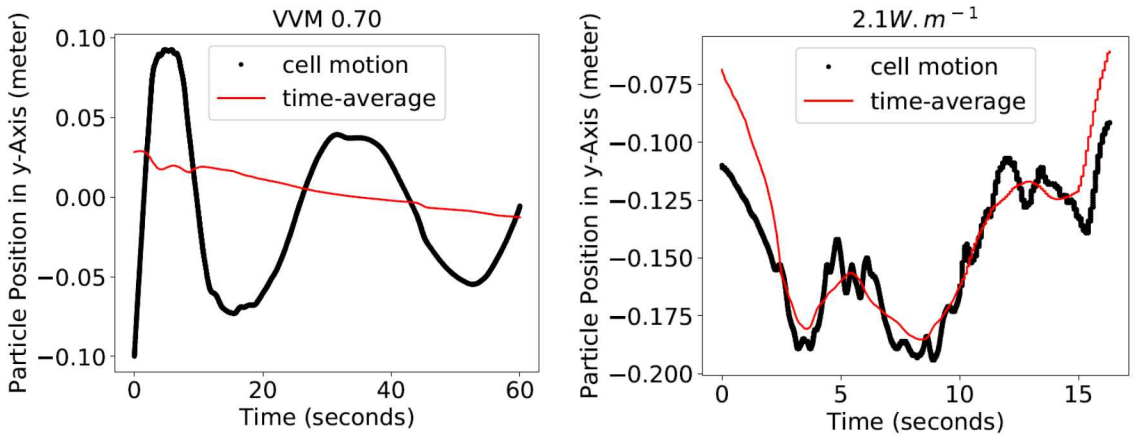

Figure A4. Photoautotrophic microorganism cell motion open raceway pond at flat-panel photobioreactor (left figure) and open raceway pond (right figure).

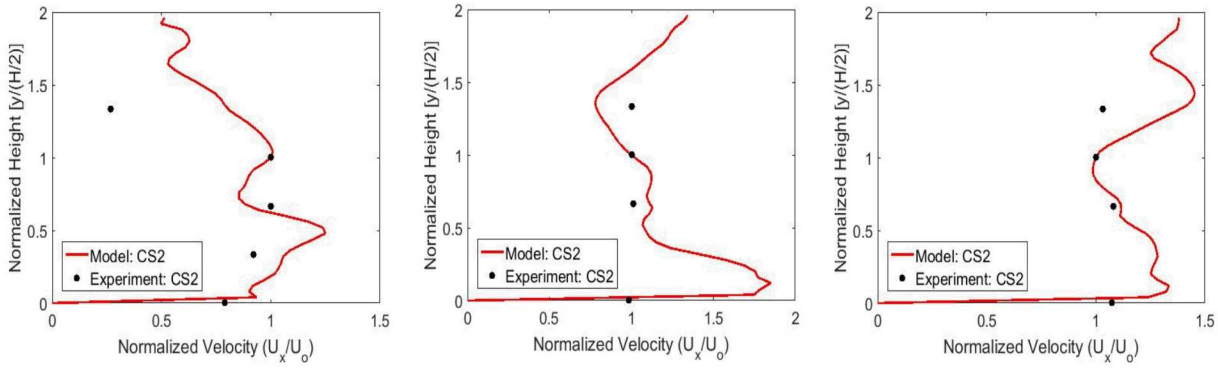

Figure A5. Validation of DNS based CFD model of open raceway pond at mixing energy inputs of 0.1 W.m-3 (left figure), 0.7 W.m-3 (middle figure) and 1.94 W.m-3 (right figure).

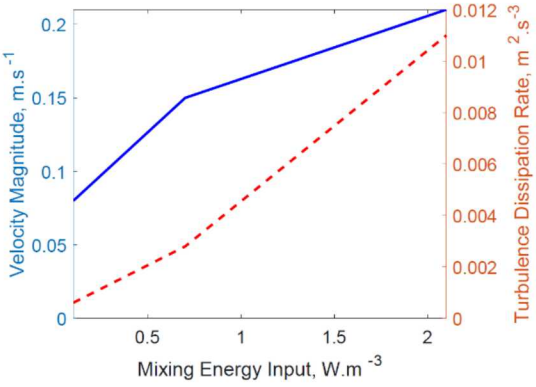

Figure A6. Experimental input velocity magnitude and turbulence dissipation rate as a function of mixing energy input in the open raceway pond.